

Enhanced visible emissions of Pr³⁺-doped oxyfluoride transparent glass-ceramics containing SrF₂ nanocrystals

C.R. Kesavulu^a, C.S. Dwaraka Viswanath^b, Sujita Karki^a, Pabitra Aryal^a, H.J. Kim^{a,*},
C.K. Jayasankar^{b,*}

^a Department of Physics, Kyungpook National University, Daegu 41566, Republic of Korea

^b Department of Physics, Sri Venkateswara University, Tirupati 517502, India



ARTICLE INFO

Keywords:

Pr³⁺-doped glass
Oxyfluoride glass-ceramics
SrF₂ nanocrystals
Optical properties
Judd-Ofelt analysis

ABSTRACT

The Pr³⁺-doped oxyfluoride transparent glass and glass-ceramic (GC) with the composition of 41SiO₂ + 10Al₂O₃ + 25.5LiF + 23SrF₂ + 0.5Pr₂O₃ were prepared and investigated their optical and luminescence properties. The formation of SrF₂ nanocrystals in GC has been confirmed by X-ray diffraction (XRD) and transmission electron micrographs (TEM). The Fourier transform infrared spectroscopy (FT-IR) studies were used to examine the network structure characteristics of silicates in the glass matrices. The XRD and TEM results suggest that the Pr³⁺ ions are progressively incorporated into the SrF₂ nanocrystals in the GC with increase in time of thermal treatment at 650 °C, corresponding to the first crystallization temperature of the glass. The obtained visible emissions of Pr³⁺-doped GC are several times enhanced than that in the glass and the lifetime of the ³P₀ level of the Pr³⁺ ions in glass and GC are found to be 7 and 12 μs, respectively. Therefore, the enhanced visible emission and lifetimes in GC are due to the incorporation of Pr³⁺ ions into the lower phonon energy of SrF₂ nanocrystals in the GCs. Moreover, the smaller difference in ionic radius between the added trivalent ions (Pr³⁺) and Sr²⁺ induces the larger enhancement of luminescence intensity in the GC. Hence, these enhanced visible luminescence properties indicate that the present glass and GC could be useful for photonic device applications.

1. Introduction

In the recent years, tremendous work have been focused on rare-earth (RE) doped glassy systems for various applications such as display devices, sensors, solid state lasers, optical amplifiers, optical communications and photovoltaics. Mainly the RE-doped glasses and glass-ceramics (GC) are used for enhancement of luminescence properties and also to develop the efficiency of solar cells by controlling the solar spectrum with spectral conversion as up/down convertors [1,2]. Transparent glass-ceramics (TGCs), which possess the collective studies of glasses and crystals are potential optical materials that compete with single crystals and glasses. Meanwhile, several experimental research works have been established that the RE ions are selectively surrounded in the fluoride crystals which are distributed in the oxide glass matrix. Oxyfluoride GCs containing low phonon fluoride nanocrystals have the advantages of low phonon environment and higher solubility to RE activators with better mechanical and chemical stability [3,4].

Initially, Wang and Ohwaki [5] in 1993, was focused on oxyfluoride GCs containing PbF₂ and CdF₂ nanocrystals which reveal the good

luminescence properties without losing transparency on the matrix but it have limitation due to toxic in nature. Recently, TGCs containing MF₂ (M = Ca, Sr, or Ba) nanocrystals have acquired rich attention due to both the economic and non-toxicity of MF₂ raw matrices [6–9]. Among the RE ions, Pr³⁺-doped glasses exhibit an important features for rich emission that covers the whole visible and near infrared regions for optical fiber amplifiers operating at O-, E-, S-, C-, and L-bands [10,11]. In recent times many researchers pay much attention on RE doped transparent glass-ceramics containing SrF₂ nanocrystals for enhanced visible and IR emissions, efficient lasers and fiber amplifiers [12–15]. Dharmiah et al. [16] reported the luminescence and energy transfer in Dy³⁺/Tb³⁺ co-doped transparent oxyfluorosilicate glass-ceramics for green emitting applications, Jiang et al. [17] studied the Er³⁺-doped TGCs containing micron-sized SrF₂ crystals for efficient 2.7 μm lasers and amplifiers and Walas et al. [18] investigated the Eu³⁺-doped tellurite glass ceramics containing SrF₂ nanocrystals to enhance emission properties in visible region for wLED phosphor applications.

In the present work, we have successfully prepared and investigated detailed spectroscopic properties for 0.5 mol% Pr³⁺-doped oxyfluoride

* Corresponding authors.

E-mail addresses: hongjoo@knu.ac.kr (H.J. Kim), ckjaya@yahoo.com (C.K. Jayasankar).

Table 1
Physical properties of Pr³⁺-doped oxyfluoride glass and glass-ceramic (GC2h).

Properties	Glass	GC2h
Thickness (cm)	0.335	0.338
Density (g/cm ³)	3.700	3.820
Concentration (mol/l)	0.5103	0.5269
Refractive index at 589.99 nm	1.593	1.594

glass and GCs containing SrF₂ nanocrystals with enhanced visible luminescence properties for photonic device applications. To the best of our knowledge, this paper reports the first investigation of Pr³⁺-doped TGCs containing SrF₂ nanocrystals.

2. Experimental details

Pr³⁺-doped oxyfluoride glass of composition (mol%) of 41SiO₂ + 10Al₂O₃ + 25.5LiF + 23SrF₂ + 0.5Pr₂O₃ was prepared by conventional melt quenching technique at a temperature of 1450 °C for 2 h using a platinum-rhodium crucible. The precursor glasses are subjected to heat treatments at 650 °C, near the onset of crystallization peak for 2 h, which is hereafter referred as GC2h. The physical properties such as density was determined by Archimedes's method using distilled water as an immersion liquid and refractive index was measured using an ellipsometer (Woollam – M-2000) at sodium wavelength (589.99 nm) and these values are given in Table 1. Differential thermal analysis (DTA) measurements were carried out on SDT Q 600, V8.3 Build 101 Differential thermal analyzer. X-ray diffraction (XRD) spectra were made with an X-ray diffractometer (Smart lab-RIGAKU) using the Cu-Kα radiation. Transmission Electron Micrographs (TEM) and selected area electron diffraction (SAED) patterns were recorded in (JEOL-TEM 2010) with an accelerating voltage of 200 kV. Fourier transform infrared spectroscopy (FT-IR) spectra were recorded on Perkin-Elmer (Frontier) spectrometer with KBr pellet technique from 2400 to 400 cm⁻¹ with spectral resolution of 0.4 cm⁻¹. Absorption spectra were measured on a UV–visible-NIR spectrophotometer (Hitachi U-3400). The excitation, emission and decay curve measurements were obtained with a Jobin Yvon (HORIBA) fluorolog-3 spectrometer using xenon flash lamp as radiation source by exciting the samples with 444 nm. All measurements were carried out at room temperature.

3. Results and discussions

3.1. DTA analysis

The DTA curve of the present oxyfluoride precursor glass sample recorded at 5 K/min is shown in Fig. 1. From DTA analysis, the glass transition temperature (T_g), the crystallization onset temperature (T_x), crystallization peak (exotherm maximum) temperature (T_c) and melting temperature (T_m) were determined from the DTA curve as 532, 655, 678 and 857 °C, respectively. The XRD analysis demonstrates that the crystallization peak T_c is ascribed to the precipitation of SrF₂ crystals for crystallization process of the present glass matrix. The glass thermal stability (ΔT = T_x - T_g) has been estimated as a difference between T_x and T_g. The ΔT value of the present oxyfluoride glass found to be 123 °C. Moreover, the larger value of ΔT (> 100 °C) of the glass can be considered as a good thermal stability [19]. However, the evaluated ΔT is not precise value owing to the absence of T_c. Hence, the Saad and Poulain [20] obtained another criterion parameter (S) to estimate more perfectly the thermal stability of the prepared glass, which reveals the resistance to devitrification after the formation of the glass and can be defined by

$$S = \frac{(T_c - T_x) \times (T_c - T_g)}{T_g} \quad (1)$$

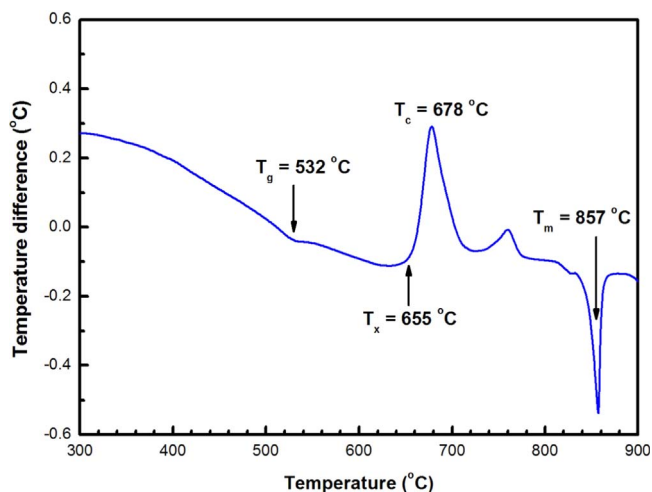


Fig. 1. DTA profile of the as-made Pr³⁺-doped oxyfluoride glass.

where (T_c-T_x) is related to the rate of devitrification transformation of the glassy phase. In addition, the high value of ΔT delays the nucleation process. In present oxyfluoride glass system, the obtained values of ΔT = 123 °C and S = 6.31 °C are found to be higher than that of other bismuth silicate glasses (ΔT = 87 °C; S = 9.41) [21], whereas lower than that of other fluorozirconate-based glass ceramics with BaF₂ nanocrystals (ΔT = 30 °C; S = 0.33 °C) [22]. The Hruby's criterion parameter (H_R), which is a numerical measure of the glass-forming tendency and it involves the T_g, T_c and T_m temperatures [23] as:

$$H_R = \frac{(T_c - T_g)}{(T_m - T_c)} \quad (2)$$

Typically, H_R values vary in between 0.1 and 2.0 for good glass forming matrices. In the present oxyfluoride glass system, the H_R value is found to be 0.82, which suggests that the present glass system is comparatively more inclination of crystallization in the SiO₂ + Al₂O₃ + LiF + SrF₂ glass-ceramics which is essentially caused by the addition of SrF₂ into precursor glass matrix with 23 mol%. However, this result indicates that it could be an advantage of preparation of glass ceramics from the precursor glass. Hence, in order to attain nanosized crystals in the glass matrix is fully dependent on the temperature and time of the heat treatment procedure based on few degrees above T_g and below the T_x temperatures [18]. Because of these two reasons in the present study, we have selected at 650 °C (below the T_x) to obtain transparent GC containing SrF₂ nanocrystalline phase.

3.2. XRD analysis

The XRD profile of glass and GC samples are shown in Fig. 2. As expected, the XRD curve of the glass contains two broad humps without the presence of any sharp diffraction peaks for the precursor glass sample and reveals the amorphous nature. On contrary, the XRD patterns of GC indicates that the presence of few narrow and relatively intense peaks are ascribed to cubic SrF₂ crystalline phase with JCPDS standard card No. 98-004-1402 with the space group of *Fm-3m* (225). With the full width at half maximum (FWHM) of diffraction peaks, the average size of GC2h sample containing cubic SrF₂ nanocrystals was obtained to be about 34 nm using the Scherrer's equation [19,24], which is comparable to that of the RE-doped GC containing SrF₂ nanocrystals [6,18].

3.3. TEM and SAED analysis

The Pr³⁺-doped GC2h sample for TEM morphology is shown in Fig. 3 (left). It shows that the almost all the particles are in clusters of

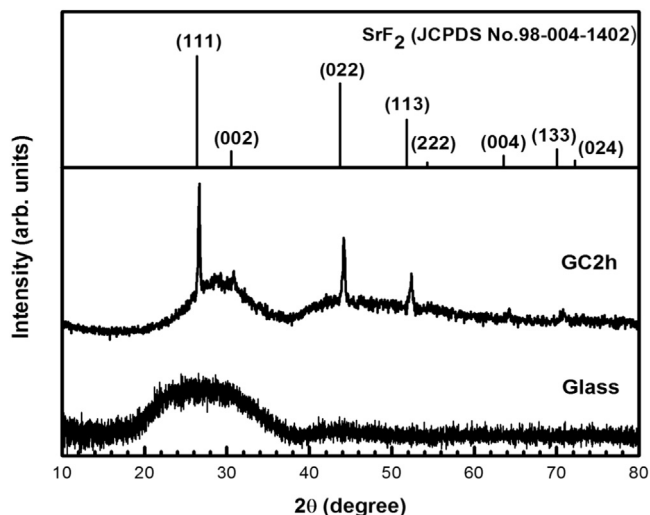


Fig. 2. XRD patterns of the Pr^{3+} -ions in glass and GC2h.

homogeneous distribution of spherical nanocrystals with dark appearance and few particles are agglomerates with an asymmetrical shape among glassy matrix. The couple of particles show nano-sized spherical-like morphology, with an average particle size of 36 nm, which was consistent with the diameter estimated by Scherrer's equation. The bright diffraction pattern rings exist from the diffraction planes of polycrystalline phase of the GC2h sample as exposed in the selected area electron diffraction pattern (SAED) and is shown in Fig. 3 (right). As seen from Fig. 3 (right), all the diffraction rings could be acknowledged appropriately as the cubic SrF_2 planes and are reliable with the XRD pattern.

3.4. FT-IR analysis

The Fig. 4 shows the FT-IR spectra of glass and GC2h samples in the spectral range of $400\text{--}2400\text{ cm}^{-1}$, which is used to study the network structure of the present oxyfluoride glass and GC2h. As can be seen from Fig. 4, the observed bands are related to characteristic of silicate group vibrations. The obtained spectra consist of the couple of strong and sharp peaks and are located at 473 cm^{-1} and are assigned to the O-Si-O bending vibration [25]. The peak at 728 cm^{-1} is ascribed to the Si-O-Si symmetric stretching vibration. The sharp and very important strong band at 1000 cm^{-1} is the characteristic absorption of silica vibration mode corresponding to the Si-O-Si symmetric stretching [26]. Moreover, the two weak absorption bands located at 1448 and 1634 cm^{-1} are due to OH-bonded to H_2O molecule coupled with a deformation mode of absorbed H_2O molecule on the sample surface

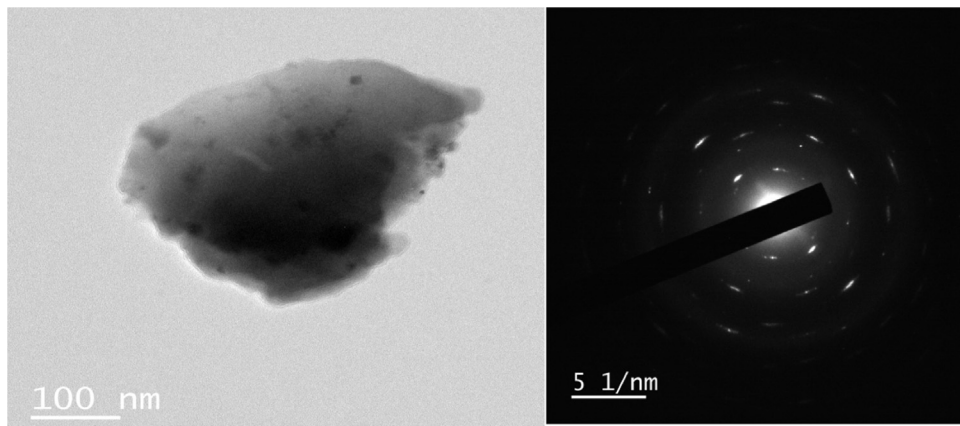


Fig. 3. TEM micrograph of the Pr^{3+} -ions in GC2h ($650\text{ }^\circ\text{C}/2\text{ h}$) with the SAED pattern.

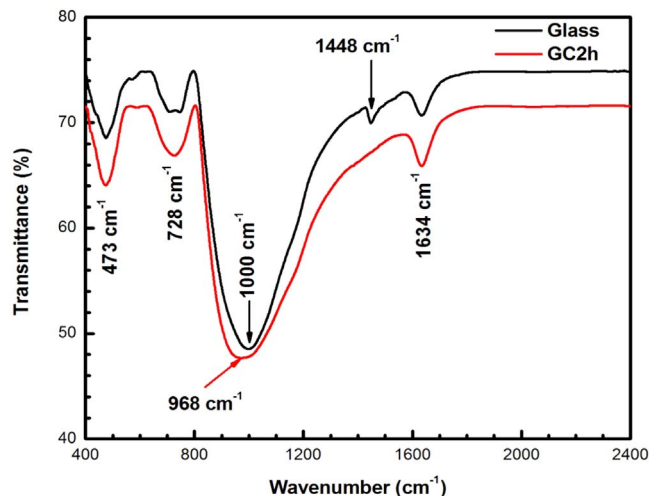


Fig. 4. FT-IR spectra of the Pr^{3+} -doped oxyfluoride glass and GC2h.

[27].

In comparison with the glass and GC2h in the FT-IR spectra, all the observed bands are possessed similar characteristics for 473 , 728 and 1634 cm^{-1} . But the band at 1448 cm^{-1} has been disappeared in the GC2h sample and it is due to the presence of fluorides in the GC2h sample that strongly reduces OH absorption and therefore the band at 1448 cm^{-1} disappears completely compared to glass sample. Another important point observed from Fig. 4 is that the maximum intensity vibration band in FT-IR spectra is considered to be phonon energy of the host glass which is decreased or shifted from 1000 cm^{-1} to 968 cm^{-1} from glass to GC2h samples. Therefore, the decreasing of phonon energy from glass to GC2h is due to the formation of SrF_2 nanocrystals in the GC2h sample [28] and in turn enhances the luminescence properties in the present SrF_2 containing transparent GCs.

3.5. Optical absorption-Judd-Ofelt analysis and radiative properties

Absorption spectra of $0.5\text{ mol}\%$ Pr^{3+} -doped oxyfluoride glass and GC in the UV-visible-NIR range ($250\text{--}2400\text{ nm}$) are shown in Fig. 5 and the inset shows the digital images of glass and GC samples. The absorption spectra exhibits six absorption bands in glass and GC, which are assigned to transitions from the $^3\text{H}_4$ ground level to several excited levels of the Pr^{3+} ions such as $^3\text{F}_2$, $^3\text{F}_3 + ^3\text{F}_4$, $^1\text{G}_4$, $^1\text{D}_2$, $^3\text{P}_{0,1} + ^1\text{I}_6$ and $^3\text{P}_2$ located at around 1925 , 1521 , 1006 , 590 , 482 and 444 nm , respectively [29,30]. From absorption spectra, the precursor glass is completely transparent but GC2h is faintly decreasing transparency. The decrease in transparency could be ascribed to light scattering by larger nanocrystals. As per the Rayleigh-Ganz particle scattering theory [31], to

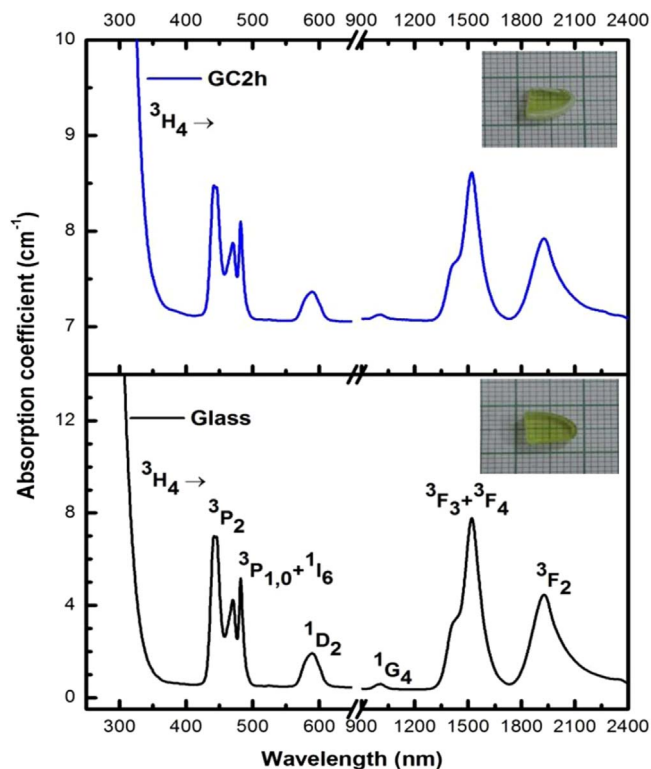


Fig. 5. Absorption spectra of the Pr^{3+} -ions in glass and GC2h.

maintain high transparency, the large grain size of nanocrystals of GCs is limited to less than the corresponding wavelength. Usually, when the size of the grains reaches the micron size level, strong light scattering in the GCs are translucent or even turbid, which indicates a poor potential for optical and luminescence applications [17]. Moreover, in glass and GC2h samples, absorption spectra exhibit an elevated baseline shift for GC2h sample. Usually, baseline shift in the absorption spectra may arise due to main reasons of reflection losses, which increases with refractive index and light scattering either from surface roughness or from any species present on the surface of the sample. Therefore, in the present GC2h sample, the baseline shift is mainly due to the enhanced scattering loss resulting from the formation of SrF_2 nanocrystals in the glass matrix rather than reflection loss [32].

The absorption band positions (λ_p), experimental (f_{exp}) and calculated (f_{cal}) oscillator strengths (10^{-6}) of Pr^{3+} -doped glass with 0.5 mol % and GC have been determined by using the relations reported in literature [33] within the framework of the Judd-Ofelt (JO) theory [34,35] and were displayed in Table 2. Convincingly small root mean square (σ_{rms}) deviations ($\times 10^{-6}$) of ± 0.84 and ± 0.21 are found for glass and GC2h, respectively, signifying the quality of the fit between the experimental and calculated oscillator strengths.

Among the absorption bands, $^3\text{H}_4 \rightarrow ^3\text{P}_2$ and $^3\text{H}_4 \rightarrow ^3\text{F}_3$ located at 444 and 1521 nm, respectively, are most intense and known as hypersensitive transitions (HSTs), which strongly depends on the local environment of the RE ions and affects the JO intensity parameters. Such HSTs are governed by a selection rules $|\Delta S| = 0$, $|\Delta L| \leq 2$, and $|\Delta J| \leq 2$ [30]. From Table 2, it is remarkable to note that oscillator strength of these HSTs is smaller in glass ceramics than that in glass. This is an indication for the higher site asymmetry of Pr^{3+} ions in the glass [36].

The JO intensity parameters (Ω_λ , $\lambda = 2, 4, 6$) have been derived [33–35] by using the experimental oscillator strengths of the observed different absorption bands and refractive index, and are displayed in Table 3. For the calculation of JO parameters, the matrix elements, $||U^\lambda||^2$, have been taken from reported literature by Carnall et al. [37]. As seen from Table 3, Ω_2 values gradually decreases from glass to GC

Table 2

The absorption band energy (cm^{-1}), experimental (f_{exp}) and calculated (f_{cal}) oscillator strengths (10^{-6}) of 0.5 mol% Pr^{3+} -doped glass and glass-ceramic (GC2h). Absorption transitions are from the $^3\text{H}_4$ ground state to the excited states along with the Judd-Ofelt intensity parameters (Ω_λ , $\times 10^{-20} \text{ cm}^2$).

Level $^3\text{H}_4 \rightarrow$	Glass			GC2h		
	Energy	f_{exp}	f_{cal}	Energy	f_{exp}	f_{cal}
$^3\text{F}_2$	5187	8.31	8.31	5192	1.60	1.60
$^3\text{F}_3 + ^3\text{F}_4$	6575	17.06	17.09	6575	3.41	3.42
$^1\text{G}_4$	9911	0.49	0.52	9921	0.09	0.10
$^1\text{D}_2$	16,964	3.79	1.91	16,964	0.85	0.38
$^3\text{P}_{0,1,2} + ^1\text{I}_6$	22,624	35.76	35.76	22,624	7.25	7.25
$\sigma(\text{N})^a$		$\pm 0.84(5)$			$\pm 0.21(5)$	
Ω_2		1.83				0.18
Ω_4		18.82				3.83
Ω_6		6.25				1.24

^a σ refers rms deviation between experimental and calculated values and N refers the number of levels used in the fit.

Table 3

The Judd-Ofelt intensity parameters (Ω_λ , $\times 10^{-20} \text{ cm}^2$) of Pr^{3+} ions in the glass and glass-ceramic (GC2h) along with other systems.

Systems	Ω_2	Ω_4	Ω_6	Trend
Glass [P.W]	1.83	18.82	6.25	$\Omega_4 > \Omega_6 > \Omega_2$
GC2h (glass-ceramic) [P.W]	0.18	3.83	1.24	$\Omega_4 > \Omega_6 > \Omega_2$
Oxyfluoride [38]	– 0.66	12.49	3.17	$\Omega_4 > \Omega_6 > \Omega_2$
MgTP [39]	2.69	11.87	8.39	$\Omega_4 > \Omega_6 > \Omega_2$
LNB [40]	2.98	6.98	4.82	$\Omega_4 > \Omega_6 > \Omega_2$
BiBO:Pr1% [29]	9.97	5.37	15.72	$\Omega_6 > \Omega_2 > \Omega_4$
$\text{La}_2\text{CaB}_{10}\text{O}_{19}$ [41]	8.63	0.97	10.12	$\Omega_6 > \Omega_2 > \Omega_4$
$\text{Sr}_3\text{Y}_2(\text{BO}_3)_4$ [41]	10.57	2.94	17.85	$\Omega_6 > \Omega_2 > \Omega_4$
$\text{Ca}_4\text{GdO}(\text{BO}_3)_3$ [42]	7.35	1.15	3.09	$\Omega_2 > \Omega_6 > \Omega_4$
KPb_2Cl_5 [43]	15.64	4.95	6.23	$\Omega_2 > \Omega_6 > \Omega_4$
CdS nanoparticles [44]	10.58	7.4	0.95	$\Omega_2 > \Omega_4 > \Omega_6$

P.W: Present work.

signifying that the bonding arrangements of Pr^{3+} ion is less covalent/more ionic in the GCs. This is due to the formation of SrF_2 nanocrystals by progressive incorporation of Pr^{3+} ions into the glass matrices. Thus the Pr^{3+} ions could be penetrated into the SrF_2 nanocrystalline phase and the Sr^{2+} ions are partially substituted by Pr^{3+} ions [6].

The JO parameters ($\times 10^{-20} \text{ cm}^2$) of glass and GC2h are $\Omega_2 = 1.83$, $\Omega_4 = 18.82$, and $\Omega_6 = 6.25$; and $\Omega_2 = 0.18$, $\Omega_4 = 3.83$, and $\Omega_6 = 1.24$, respectively. These values are compared with other Pr^{3+} -doped glasses, crystals and nanoparticle in Table 3 that includes oxyfluoride [38], MgTP [39], LNB [40] and BiBO:Pr1% [29] glasses, $\text{La}_2\text{CaB}_{10}\text{O}_{19}$ [41], $\text{Sr}_3\text{Y}_2(\text{BO}_3)_4$ [41], $\text{Ca}_4\text{GdO}(\text{BO}_3)_3$ [42] and KPb_2Cl_5 [43] crystals and CdS nanoparticles [44]. The trend of JO intensity parameters ($\Omega_4 > \Omega_6 > \Omega_2$) is similar for glass and GC2h (glass-ceramic), oxyfluoride [38], MgTP [39] and LNB [40] systems whereas for other Pr^{3+} -doped BiBO:Pr1% [29], $\text{La}_2\text{CaB}_{10}\text{O}_{19}$ [41] and $\text{Sr}_3\text{Y}_2(\text{BO}_3)_4$ [41] systems are follow the JO trend as $\Omega_6 > \Omega_2 > \Omega_4$. The Pr^{3+} -doped KPb_2Cl_5 [43] follow the JO trend as $\Omega_2 > \Omega_6 > \Omega_4$ and Pr^{3+} -doped CdS nanoparticles [44] follow the general JO trend as $\Omega_2 > \Omega_4 > \Omega_6$. This trend of variations in JO intensity parameters are due to the high and very sensitive values of two HSTs oscillator strengths. The Ω_4 parameter is affected by the factor causing changes in both Ω_2 and Ω_6 and is not usually studied for local structure investigations [45,46].

The JO parameters have been used to predict radiative lifetimes (τ_R) for $^3\text{P}_1$, $^3\text{P}_0$, $^1\text{D}_2$ and $^3\text{F}_3$ levels of Pr^{3+} in glass and GC2h and are presented in Table 4. As seen from Table 4, the τ_R values for the present glass and GC2h follows the similar trend as $^3\text{F}_3 > ^1\text{D}_2 > ^3\text{P}_1 > ^3\text{P}_0$. A similar trend was also found for Pr^{3+} -doped SLBiBPr05 [47] glass. These τ_R values decreases incessantly with increase of the higher level energies. Therefore, the τ_R values in the studied glass and GC2h are comparable to other Pr^{3+} -doped systems [38,43,47–50] as shown in

Table 4

Comparison of predicted radiative decay times (τ_r , μs) of some important luminescence levels of Pr^{3+} doped glass and GC2h along with reported Pr^{3+} -doped systems.

S.No.	Excited level	Glass [P.W]	GC2h [P.W]	SLBiBPr05 [47]	Oxyfluoride [38]	KPb ₂ Cl ₅ [43]	NaZBS [48]	PbO-PbF ₂ [49]	CaBPr [50]
1	³ P ₁	10.3	52.1	5.0	–	–	6.2	15	12.9
2	³ P ₀	9.5	48.2	4.8	14	8.2	6.0	14	47.5
3	¹ D ₂	169.5	895.8	49.8	298	85	65.7	252	193.2
4	³ F ₃	670.2	3375.0	216.2	–	501	–	–	–

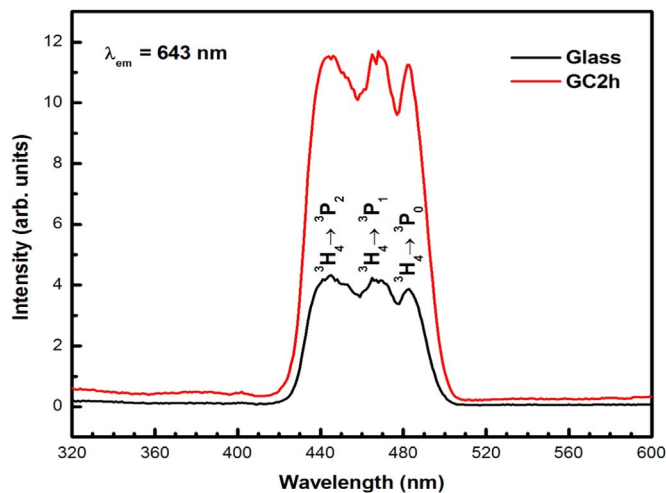
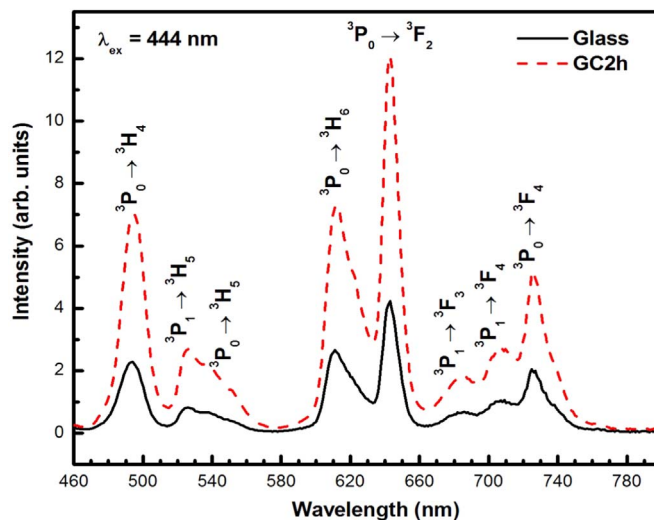
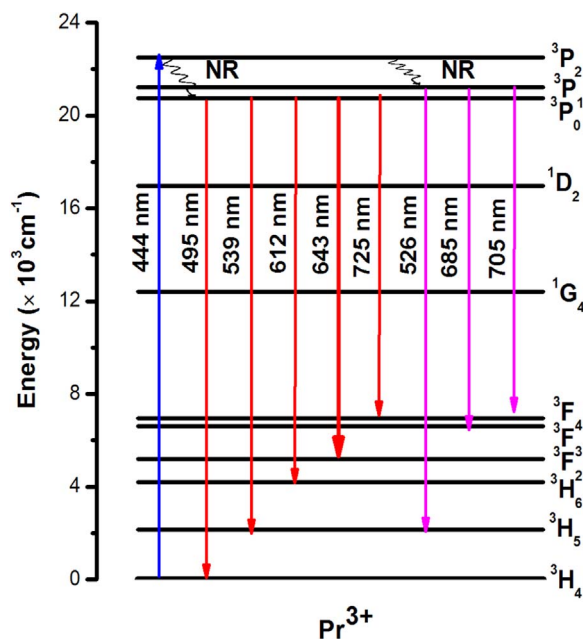
Fig. 6. Excitation spectra ($\lambda_{em} = 643 \text{ nm}$) of the Pr^{3+} -ions in glass and GC2h.Fig. 7. Emission spectra ($\lambda_{ex} = 444 \text{ nm}$) of the Pr^{3+} -ions in glass and GC2h.

Table 4.

3.6. Excitation and emission spectra analysis

Emission properties of the glass and GC doped with Pr^{3+} ions are explored in order to verify the effect of Pr^{3+} ions and surroundings with SrF_2 containing nanocrystals for enhancement of emission intensities from glass to GC. Fig. 6 shows the excitation spectra of Pr^{3+} -doped oxyfluoride glass and GC2h monitored at 643 nm. As seen from Fig. 6, three bands are observed at 444, 468 and 483 nm from excitation spectra, and are in good agreement with absorption spectra, corresponding to the transitions from the $^3\text{H}_4 \rightarrow ^3\text{P}_2$, $^3\text{H}_4 \rightarrow ^3\text{P}_1$ and $^3\text{H}_4 \rightarrow ^3\text{P}_0$ of Pr^{3+} ions, respectively, those are similar for glass and GC2h. Among the three excitations, the intense and strong excitation band at 444 nm ($^3\text{H}_4 \rightarrow ^3\text{P}_2$) is used to investigate the emission spectra characteristics for the present Pr^{3+} -doped glass and GC samples.

The visible emission spectra of glass and GC2h samples are measured with an excitation at 444 nm and are shown in Fig. 7. As seen from Fig. 7, emission spectra consist of eight characteristic emission bands of Pr^{3+} ions at 495, 526, 539, 612, 643, 685, 705 and 726 nm, assigned to the electronic transitions of $^3\text{P}_0 \rightarrow ^3\text{H}_4$, $^3\text{P}_1 \rightarrow ^3\text{H}_5$, $^3\text{P}_0 \rightarrow ^3\text{H}_5$, $^3\text{P}_0 \rightarrow ^3\text{H}_6$, $^3\text{P}_0 \rightarrow ^3\text{F}_2$, $^3\text{P}_1 \rightarrow ^3\text{F}_3$, $^3\text{P}_1 \rightarrow ^3\text{F}_4$ and $^3\text{P}_0 \rightarrow ^3\text{F}_4$, respectively. Typically, Pr^{3+} -doped glass systems may exhibit emission transitions of $^1\text{D}_2 \rightarrow ^3\text{H}_4$ (orange) and $^3\text{P}_0 \rightarrow ^3\text{H}_6$ (red) in red spectral range 580–640 nm. Due to the superposition of the peaks associated with $^1\text{D}_2 \rightarrow ^3\text{H}_4$ (~ 602 nm) and $^3\text{P}_0 \rightarrow ^3\text{H}_6$ (~ 612 nm) transitions of Pr^{3+} ions, it may not be possible to locate and assign these two transitions more accurately and separately. Also, the relative intensities of these two transitions are found to be very sensitive to the Pr^{3+} ion concentrations as well as multi-phonon relaxation phenomenon involved [51,52]. However, for example, the $^1\text{D}_2 \rightarrow ^3\text{H}_4$ transition appears as a shoulder to the dominant $^3\text{P}_0 \rightarrow ^3\text{H}_6$ transition [10,39,51,53,57]. Some of them reported only $^3\text{P}_0 \rightarrow ^3\text{H}_6$ [29,52,54,56,58] and $^1\text{D}_2 \rightarrow ^3\text{H}_4$ transition [11,30,47]. In the present study, as can be seen from the Fig. 7, the $^1\text{D}_2 \rightarrow ^3\text{H}_4$ (orange) transition was not observed both in the Pr^{3+} -doped glass and GC2h systems.

Fig. 8. Partial energy level diagram of Pr^{3+} ions in oxyfluoride glass and GC.

These emission channels are displayed in the partial energy level diagram (Fig. 8) of Pr^{3+} ions in glass and GC. As seen from Fig. 7, it is noted that the intensities of visible emission for GC2h sample was several times significantly enhanced than that in precursor glass.

The overall enhancement in visible emission in GC2h sample is owing to reduction of phonon energy of the host glass (see Fig. 4) which minimize multiphonon relaxation rate between energy levels of the doping of Pr^{3+} ions into SrF_2 nanocrystals. Moreover, the enhancement of visible luminescence intensity in the GC2h sample might be the smaller difference in ionic radius between the added trivalent Pr^{3+}

Table 5

Emission peak wavelengths (λ_p , nm), effective bandwidths ($\Delta\lambda_{\text{eff}}$, nm), experimental decay time (τ_{exp} , μs) and stimulated emission cross-sections ($\sigma(\lambda_p)$, $\times 10^{-20} \text{ cm}^2$) of Pr^{3+} -doped glass and GC2h along with reported Pr^{3+} -doped systems.

System	Transition	λ_p	$\Delta\lambda_{\text{eff}}$	τ_{exp}	$\sigma(\lambda_p)$
Glass [P.W]	$^3\text{P}_0 \rightarrow ^3\text{H}_4$	495	16.57	–	14.38
	$^3\text{P}_0 \rightarrow ^3\text{H}_6$	612	20.83	–	1.87
	$^3\text{P}_0 \rightarrow ^3\text{F}_2$	643	11.07	7.0	4.33
GC2h [P.W]	$^3\text{P}_0 \rightarrow ^3\text{H}_4$	495	16.02	–	3.03
	$^3\text{P}_0 \rightarrow ^3\text{H}_6$	612	22.57	–	0.34
	$^3\text{P}_0 \rightarrow ^3\text{F}_2$	643	11.06	12.0	0.43
GBT:G [56]	$^3\text{P}_0 \rightarrow ^3\text{H}_6$	614	25	6.2	114
	$^3\text{P}_0 \rightarrow ^3\text{F}_2$	647	11	7.2	275
GBT:GC [56]	$^3\text{P}_0 \rightarrow ^3\text{H}_6$	614	27	7.8	96.7
	$^3\text{P}_0 \rightarrow ^3\text{F}_2$	647	13	9.3	203.2
SAPCF:G [57]	$^3\text{P}_0 \rightarrow ^3\text{H}_4$	483	–	4.3	2.81
	$^3\text{P}_0 \rightarrow ^3\text{F}_2$	633	–	–	17.33
SAPCF:GC [57]	$^3\text{P}_0 \rightarrow ^3\text{H}_4$	489	–	5.3	4.95
	$^3\text{P}_0 \rightarrow ^3\text{F}_2$	633	–	–	29.8
	$^3\text{P}_0 \rightarrow ^3\text{F}_2$	640	–	10.0	–
TZYN:G [58]	$^3\text{P}_0 \rightarrow ^3\text{F}_2$	640	–	15.0	–
TZYN:GC6 [58]	$^3\text{P}_0 \rightarrow ^3\text{F}_2$	640	–	11.0	–
TZYN:GC10 [58]	$^3\text{P}_0 \rightarrow ^3\text{F}_2$	640	–	–	–
AG-0 [7]	$^3\text{P}_0 \rightarrow ^3\text{H}_4$	485	–	12.3	–
AG-1 [7]	$^3\text{P}_0 \rightarrow ^3\text{H}_4$	485	–	7.2	–
GC-1 [7]	$^3\text{P}_0 \rightarrow ^3\text{H}_4$	485	–	7.0	–

(0.99 Å) ions and Sr^{2+} (1.13 Å) ions in the GC containing SrF_2 nanocrystals [32,55]. From emission spectra, the emission peak wavelengths (λ_p), effective bandwidths ($\Delta\lambda_{\text{eff}}$) and stimulated emission cross-sections ($\sigma(\lambda_p)$) of Pr^{3+} -doped glass and GC for the important emission transitions have been determined and are presented in Table 5 along with some other reported Pr^{3+} -doped systems that include 0.1 PrF_3 + 2.9 GdF_3 + 32 SrF_2 + 42 SiO_2 + 23 Al_2O_3 (AG-0) [7], 0.1 PrF_3 + 1.0 YbF_3 + 1.9 GdF_3 + 32 SrF_2 + 42 SiO_2 + 23 Al_2O_3 (AG-1) [7], 0.1 PrF_3 + 1.0 YbF_3 + 1.9 GdF_3 + 32 SrF_2 + 42 SiO_2 + 23 Al_2O_3 (heat treated at 610 °C for 4 h; (GC-1)) [7], 54 GeO_2 + 30 BaO + 15 TiO_2 + 1.0 Pr_6O_{11} (GBT:G) [56], 54 GeO_2 + 30 BaO + 15 TiO_2 + 1.0 Pr_6O_{11} [heat treated at 720 °C for 3 h] (GBT:GC) [56], 29.4 SiO_2 + 18.0 Al_2O_3 + 12.0 P_2O_5 + 20.0 CaCO_3 + 18.0 CaF_2 + 0.3 La_2O_3 + 0.5 Li_2CO_3 + 0.3 B_2O_3 + 0.5 ZrO_2 + 0.33 Pr_6O_{11} (SAPCF:G) [57], 29.4 SiO_2 + 18.0 Al_2O_3 + 12.0 P_2O_5 + 20.0 CaCO_3 + 18.0 CaF_2 + 0.3 La_2O_3 + 0.5 Li_2CO_3 + 0.3 B_2O_3 + 0.5 ZrO_2 + 0.33 Pr_6O_{11} [heat treated at 790 °C for 24 h] (SAPCF:GC) [57], 49.5 TeO_2 + 30 ZnO + 10 YF_3 + 10 NaF + 0.5 Pr_2O_3 (TZYN:G) [58], 48.5 TeO_2 + 30 ZnO + 10 YF_3 + 10 NaF + 0.5 Pr_2O_3 + 1.0 AgNO_3 [heat treated at 300 °C for 6 h] (TZYN:GC6) [58] and 48.5 TeO_2 + 30 ZnO + 10 YF_3 + 10 NaF + 0.5 Pr_2O_3 + 1.0 AgNO_3 [heat treated at 300 °C for 10 h] (TZYN:GC10) [58]. As can be seen from Table 5, the $\sigma(\lambda_p)$ values are comparable to other reported Pr^{3+} -doped systems [56,57].

3.7. Decay time analysis

The decay curves of the $^3\text{P}_0$ level in glass and GC2h are recorded by exciting at 444 nm and detecting the emission at 643 nm and are shown in Fig. 9. The decay curves are found to be non-exponential nature for both the glass and GC2h samples. The non-exponential decay curves are well fitted for $^3\text{P}_0 \rightarrow ^3\text{F}_2$ level by using the following expression given as [59]

$$I(t) = A_1 \exp\left(-\frac{t}{\tau_1}\right) + A_2 \exp\left(-\frac{t}{\tau_2}\right) \quad (3)$$

where $I(t)$ is the emission intensity, τ_1 and τ_2 are the short and long decay times, A_1 and A_2 are constants, respectively. The experimental average decay times of the present glass and GC samples can be determined by using the following formula:

$$\tau_{\text{avg}} = \frac{A_1 \tau_1^2 + A_2 \tau_2^2}{A_1 \tau_1 + A_2 \tau_2} \quad (4)$$

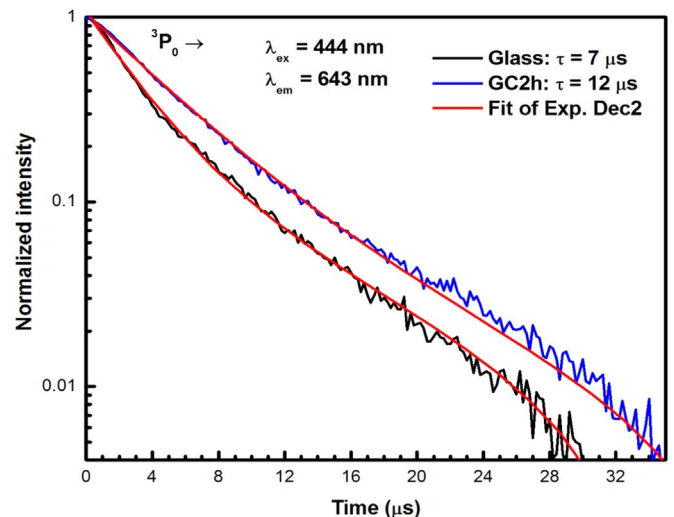


Fig. 9. Decay curves of the $^3\text{P}_0$ emitting level of the Pr^{3+} ions in glass and GC2h.

The average lifetimes (τ_{avg}) are estimated to be 7.0 and 12.0 μs for glass and GC2h, respectively. Fluorescence decay times of RE ions mainly depend on their incorporation of coordination numbers and the phonon energy. The phonon energy is reduced by tightly bounded atoms in a crystal structure and in turn the decay times of the excited level can be enhanced [60]. Hence, these results obviously specify that the doping of Pr^{3+} ions into SrF_2 nanocrystals in the GC2h sample enhances the decay time of the $^3\text{P}_0$ level. The obtained decay times of the present glass and GC2h samples are comparable to that of Pr^{3+} -doped transparent GBT glass and GC [56], Pr^{3+} -doped oxyfluoride GCs containing SrF_2 nanocrystals [7], and Pr^{3+} ions in TZYN glasses contain silver ions and nanoparticles [58].

4. Conclusions

Pr^{3+} -doped transparent oxyfluoride GC containing SrF_2 nanocrystals were synthesized and characterized their optical, structural and luminescence properties. The formation of SrF_2 nanocrystals was confirmed by XRD patterns and the average size of SrF_2 nanocrystal was found to be 34 nm. The Judd-Ofelt intensity parameters progressively decrease from glass to GCs signifying that the typical change of surroundings nearby the Pr^{3+} ions from oxide to fluoride. The obtained visible emissions of Pr^{3+} -doped GC are several times enhanced than that in the glass. The decay times of the $^3\text{P}_0$ state of the Pr^{3+} ions in the GCs is established larger than that of glass appropriate to the doping of Pr^{3+} ions into the lower phonon energy SrF_2 nanocrystals in the GC. Moreover, the smaller difference in ionic radius between the added trivalent ions (Pr^{3+}) and Sr^{2+} induces the larger enhancement of luminescence intensity in the GC. Hence, the above results clearly show the enhanced visible luminescence properties and it indicates that the present glass and GC could be useful for photonic device applications.

Acknowledgments

These investigations have been funded by the Ministry of Science and Technology, Korea (MEST) (No.2015R1A2A1A13001843). One of the authors (CKJ) is also highly grateful to DAE-BRNS, Mumbai, Government of India for the sanction of Mega Research Project (No.2009/34/36/BRNS/3174) under MoU between Sri Venkateswara University, Tirupati and RRCAT, Indore and BARC, Mumbai.

References

- [1] Z. Liu, B. Mei, J. Song, G. Yi, Influence of Yb concentration on the optical properties of CaF_2 transparent ceramics codoped with Er and Yb, *J. Am. Ceram. Soc.* 98 (2015)

- 3905–3910.
- [2] V.D. Rodriguez, V.K. Tikhomirov, J.M. Ramos, A.B. Seddon, The shape of the 1.55 μm emission band of the Er^{3+} -dopant in oxyfluoride nano-scaled glass-ceramics, *Europhys. Lett.* 69 (2005) 128–134.
- [3] M.J. Dejneka, Transparent oxyfluoride glass ceramics, *MRS Bull.* 23 (1998) 57–62.
- [4] T. Honma, M. Kusatsugu, T. Komatsu, Synthesis of LaF_3 nanocrystals by laser-induced Nd^{3+} atom heat processing in oxyfluoride glasses, *Mater. Chem. Phys.* 113 (2009) 124–129.
- [5] Y.H. Wang, J. Ohwaki, New transparent vitroceraic codoped with Er^{3+} and Yb^{3+} for efficient frequency upconversion, *Appl. Phys. Lett.* 63 (1993) 3268–3270.
- [6] C.R. Kesavulu, Mi-Yeon Yoo, Jin-Ho Lee, Ki-Soo Lim, P. Dharmiah, C.K. Jayasankar, P. Babu, Optical and upconversion properties of Er^{3+} -doped oxyfluoride transparent glass-ceramics containing SrF_2 nanocrystals, *J. Mater. Res.* 28 (2013) 1481–1489.
- [7] Y. Katayama, S. Tanabe, Mechanism of quantum cutting in Pr^{3+} - Yb^{3+} codoped oxyfluoride glass ceramics, *J. Lumin.* 134 (2013) 825–829.
- [8] J. Cai, X. Wei, F. Hu, Z. Cao, L. Zhao, Y. Chen, C. Duan, M. Yin, Up-conversion luminescence and optical thermometry properties of transparent glass ceramics containing CaF_2 : Yb^{3+} / Er^{3+} nanocrystals, *Ceram. Int.* 42 (2016) 13990–13995.
- [9] Z. Zhao, C. Liu, M. Xia, Q. Yin, X. Zhao, J. Han, Intense $\sim 1.2 \mu\text{m}$ emission from Ho^{3+} / Y^{3+} ions co-doped oxyfluoride glass-ceramics containing BaF_2 nanocrystals, *J. Alloy. Compd.* 701 (2017) 392–398.
- [10] J. Pisarska, W.A. Pisarski, D. Dorosz, J. Dorosz, Spectral analysis of Pr^{3+} doped germanate glasses modified by BaO and BaF_2 , *J. Lumin.* 171 (2016) 138–142.
- [11] P. Suthanthirakumar, Ch Basavapoornima, K. Marimuthu, Effect of Pr^{3+} ions concentration on the spectroscopic properties of zinc telluro-fluoroborate glasses for laser and optical amplifier applications, *J. Lumin.* 187 (2017) 392–402.
- [12] Q. Luo, X. Qiao, X. Fan, X. Zhang, Preparation and luminescence properties of Ce^{3+} and Tb^{3+} co-doped glasses and glass ceramics containing SrF_2 nanocrystals, *J. Non-Cryst. Solids* 356 (2010) 2875–2879.
- [13] X. Wang, J. Chen, J. Li, H. Guo, Preparation and luminescence properties of Eu-doped transparent glass-ceramics containing SrF_2 nanocrystals, *J. Non-Cryst. Solids* 357 (2011) 2290–2293.
- [14] W. Huiyun, Y.E. Song, L.I.U. Tianhua, L.I. Song, H.U. Rongxuan, W. Deping, Influence of local phonon energy on quantum efficiency of Tb^{3+} - Yb^{3+} co-doped glass ceramics containing fluoride nanocrystals, *J. Rare Earth* 33 (2015) 524–528.
- [15] M.H. Imanieh, I.R. Martin, A. Nadarajah, J.G. Lawrence, V. Lavin, J. Gonzalez-Platas, Upconversion emission of a novel glass ceramic containing Er^{3+} , Yb^{3+} : $\text{Sr}_{1-x}\text{Y}_x\text{F}_{2+x}$ nano-crystals, *J. Lumin.* 172 (2016) 201–207.
- [16] P. Dharmiah, C.S. Dwaraka Viswanath, Ch Basavapoornima, K.V. Krishnaiah, C.K. Jayasankar, S.-J. Hong, Luminescence and energy transfer in Dy^{3+} / Tb^{3+} co-doped transparent oxyfluoride glass-ceramics for green emitting applications, *Mater. Res. Bull.* 83 (2016) 507–514.
- [17] Y. Jiang, J. Fan, B. Jiang, X. Mao, J. Tang, Y. Xu, S. Dai, L. Zhang, Er^{3+} -doped transparent glass ceramics containing micron-sized SrF_2 crystals for 2.7 μm emissions, *Sci. Rep.* 6 (2016) 29873–29878.
- [18] M. Walas, T. Lewandowski, A. Synak, M. Lapinski, W. Sadowski, B. Koscielska, Eu^{3+} doped tellurite glass ceramics containing SrF_2 nanocrystals: preparation, structure and luminescence properties, *J. Alloy. Compd.* 696 (2017) 619–626.
- [19] H. Chen, Y.H. Liu, Y.F. Zhou, Z.H. Jiang, Spectroscopic properties of Er^{3+} -doped tellurite glass for 1.55 μm optical amplifier, *J. Alloy. Compd.* 397 (2005) 286–290.
- [20] M. Saad, M. Poulin, Glass forming ability criterion, *Mater. Sci. Forum* 19–20 (1987) 11–18.
- [21] C. Tian, X. Chen, Y. Shuibao, Concentration dependence of spectroscopic properties and energy transfer analysis in Nd^{3+} doped bismuth silicate glasses, *Solid State Sci.* 48 (2015) 171–176.
- [22] C. Pablick, B. Ahrens, B. Henke, J.A. Johnsson, S. Schweizer, Differential scanning calorimetry investigations on Eu-doped fluorozirconate-based glass ceramics, *J. Non-Cryst. Solids* 356 (2010) 3085–3089.
- [23] A. Hruby, Evaluation of glass-forming tendency by means of DTA, *Czech. J. Phys. B* 22 (1972) 1187–1193.
- [24] A. Dwivedi, C. Joshi, S.B. Rai, Effect of heat treatment on structural, thermal and optical properties of Eu^{3+} doped tellurite glass: formation of glass-ceramic and ceramics, *Opt. Mater.* 45 (2015) 202–208.
- [25] C. Lin, Y. Song, F. Gao, H. Zhang, Y. Sheng, K. Zheng, Z. Shi, X. Xu, H. Zou, Synthesis and luminescence properties of Eu (III)-doped silica nanorods based on the sol-gel process, *J. Sol-Gel Sci. Technol.* 69 (2014) 536–543.
- [26] T.G.V.M. Rao, A. Rupesh Kumar, M. Rami Reddy, Spectroscopic studies of tungsten ions in PbO - PbF_2 - SiO_2 glasses, *J. Non-Cryst. Solids* 358 (2012) 25–29.
- [27] C.R. Kesavulu, V.B. Sreedhar, C.K. Jayasankar, Kiwan Jang, Dong-Soo Shin, S.S. Yi, Structural, thermal and spectroscopic properties of highly Er^{3+} -doped novel oxyfluoride glasses for photonic application, *Mater. Res. Bull.* 51 (2014) 336–344.
- [28] R. Narro-Garcia, H. Desirena, T. Lopez-Luke, J. Guerrero-Contreras, C.K. Jayasankar, R. Quintero-Torres, E. De la Rosa, Spectroscopic properties of Eu^{3+} / Nd^{3+} co-doped phosphate glasses and opaque glass-ceramics, *Opt. Mater.* 46 (2015) 34–39.
- [29] L.R. Jaroszewicz, A. Majchrowski, M.G. Brik, N. Alzayed, W. Kuznik, I.V. Kityk, S. Klosowicz, Specific features of fluorescence kinetics of Pr^{3+} doped BiB_3O_6 glasses, *J. Alloy. Compd.* 538 (2012) 220–223.
- [30] N. Deopa, A.S. Rao, Sk Mahamuda, M. Gupta, M. Jayasimhadri, D. Haranath, G. Vijaya Prakash, Spectroscopic studies of Pr^{3+} doped lithium lead alumino borate glasses for visible reddish orange luminescent device applications, *J. Alloy. Compd.* 708 (2017) 911–921.
- [31] M. Kerker, *The Scattering of Light and Other Electromagnetic Radiation*, Academic Press, New York, London, 1969, pp. 256–619.
- [32] K. Biswas, S. Balaji, D. Ghosh, K. Annapura, Enhanced NIR to green up-conversion from Er^{3+} -doped oxyfluoride glass and glass-ceramics containing BaGdF_5 nanocrystals, *Int. J. Appl. Glass Sci.* 8 (2017) 204–215.
- [33] P. Babu, C.K. Jaysankar, Spectroscopic of Pr^{3+} ions in lithium borate and lithium fluoroborate glasses, *Physica B* 301 (2001) 326–340.
- [34] B.R. Judd, Optical absorption intensities of rare-earth ions, *Phys. Rev. B* 127 (1962) 750–761.
- [35] G.S. Ofelt, Intensities of crystal spectra of rare-earth ions, *J. Chem. Phys.* 37 (1962) 511–520.
- [36] G. Dominiak-Dzik, Praseodymium doped NaYF_4 nanocrystals in oxyfluoride glass-ceramics; morphological and spectroscopic studies, *J. Nanosci. Nanotechnol.* 9 (2009) 2525–2531.
- [37] W.T. Carnall, P.R. Fields, K. Rajnak, Electronic energy levels in the trivalent lanthanide aquo ions. I. Pr^{3+} , Nd^{3+} , Pm^{3+} , Sm^{3+} , Dy^{3+} , Ho^{3+} , Er^{3+} , and Tm^{3+} , *J. Chem. Phys.* 49 (1968) 4424–4442.
- [38] B. Klimesz, G. Dominiak-Dzik, M. Zelechower, W. Ryba-Romanowski, Optical study of GeO_2 - PbO - PbF_2 oxyfluoride glass singly doped with Pr^{3+} , Nd^{3+} , Sm^{3+} and Eu^{3+} , *J. Alloy. Compd.* 403 (2005) 76–85.
- [39] D.V.R. Murthy, B.C. Jamalalaih, T. Sasikala, L. Rama Moorthy, M. Jayasimhadri, Kiwan Jang, H.S. Lee, S.S. Yi, J.H. Jeong, Optical absorption and emission characteristics of Pr^{3+} -doped RTP glasses, *Physica B* 405 (2010) 1095–1100.
- [40] L. Srinivasa Rao, M. Srinivasa Reddy, M.V. Ramana Reddy, N. Veeraiiah, Spectroscopic features of Pr^{3+} , Nd^{3+} , Sm^{3+} and Er^{3+} ions in Li_2O - MO (Nb_2O_5 , MoO_3 and WO_3)- B_2O_3 glass systems, *Physica B* 403 (2008) 2542–2556.
- [41] A.M. El-Naggar, N.S. Alzayed, A. Majchrowski, L. Jaroszewicz, M.G. Brik, W. Kuznik, I.V. Kityk, Preparation and fluorescence properties of $\text{La}_2\text{CaB}_{10}\text{O}_{19}$ crystals, *J. Cryst. Growth* 334 (2011) 122–125.
- [42] A. Brenier, I.V. Kityk, Spectroscopic properties of Pr^{3+} -doped $\text{Ca}_4\text{GdO}(\text{BO}_3)_3$ (GdCOB), *J. Appl. Phys.* 90 (2001) 232–236.
- [43] A. Ferrier, M. Velazquez, J.-L. Doualan, R. Moncorge, Midinfrared luminescence properties and laser potentials of Pr^{3+} doped KPr_2Cl_5 and CsCdBr_3 , *J. Appl. Phys.* 104 (2008) 123513–123514.
- [44] L. Bokatail, S. Rai, Optical properties and up-conversion of Pr^{3+} doped CdS nanoparticles in sol-gel glasses, *J. Lumin.* 130 (2010) 1857–1862.
- [45] H.E. Heidepriem, D. Ehrh, M. Bettinelli, A. Speghini, Effect of glass composition on Judd-Ofelt parameters and radiative decay rates of Er^{3+} in fluoride phosphate and phosphate glasses, *J. Non-Cryst. Solids* 240 (1998) 66–78.
- [46] A.A. Kaminskii, *Laser crystal: Their Physics and Properties*, Springer-Verlag, Berlin Heidelberg, New York, 1990.
- [47] D. Rajesh, A. Balakrishna, M. Seshadri, Y.C. Ratnakaram, Spectroscopic investigations on Pr^{3+} and Nd^{3+} doped strontium-lithium-bismuth borate glasses, *Spectrochim. Acta A* 97 (2012) 963–974.
- [48] C.K. Jayasankar, V.V. Ravi Kanth Kumar, Judd-Ofelt intensity analysis and spectral studies of Pr^{3+} (III) ions in alkali zinc borosulphate glasses, *Mater. Chem. Phys.* 46 (1996) 84–91.
- [49] P. Nachimuthu, R. Jagannathan, Absorption and emission spectral studies of Pr^{3+} and Tm^{3+} ions in PbO - PbF_2 glasses, *Phys. Chem. Glasses* 36 (1995) 77–81.
- [50] J. Anjiah, C. Laxmikanth, N. Veeraiiah, P. Kistaiah, Luminescence properties of Pr^{3+} doped Li_2O - MO - B_2O_3 glasses, *J. Lumin.* 161 (2015) 147–153.
- [51] Bozena Burtan-Gwizdala, Manuela Reben, Jan Cisowski, Radoslaw Lisiecki, Witold Ryba-Romanowski, Bozena Jarzabek, Zbigniew Mazurak, Natalia Nosidlak, Iwona Grelowska, The influence of Pr^{3+} content on luminescence and optical behavior of TeO_2 - WO_3 - PbO - Lu_2O_3 glass, *Opt. Mater.* 47 (2015) 231–236.
- [52] M.P. Belancon, J.D. Marconi, M.F. Ando, L.C. Barbosa, Near-IR emission in Pr^{3+} single doped and tunable near-IR emission in Pr^{3+} / Yb^{3+} codoped tellurite glasses for broadband optical amplifiers, *Opt. Mater.* 36 (2014) 1020–1026.
- [53] L.R.P. Kassab, C.B. de Araujo, R.A. Kobayashi, R. de Almeida Pinto, D.M. da Silva, Influence of silver nanoparticles in the luminescence efficiency of Pr^{3+} -doped tellurite glasses, *J. Appl. Phys.* 102 (2007) 103515–4.
- [54] E.A.F. Santos, W.F. Silva, M.T. de Araujo, M.V.D. Vermelho, I. Guedes, C.-K. Loong, L.A. Boatner, C. Jacinto, Quantum efficiencies and thermo-optical properties of Er^{3+} -, Nd^{3+} -, and Pr^{3+} -single doped lead-indium-phosphate glasses, *J. Appl. Phys.* 106 (2009) 113111–113116.
- [55] S. Okamoto, H. Yamamoto, Emission from BaTiO_3 : Pr^{3+} controlled by ionic radius of added trivalent ion, *J. Appl. Phys.* 91 (2002) 5492–5494.
- [56] G. Lakshminarayana, H. Yang, Y. Teng, J. Qiu, Spectral analysis of Pr^{3+} -, Sm^{3+} - and Dy^{3+} -doped transparent GeO_2 - BaO - TiO_2 glass ceramics, *J. Lumin.* 129 (2009) 59–68.
- [57] J. Huang, S. Zhang, Y. Chen, X. Gong, Y. Lin, Z. Luo, Y. Huang, Spectral properties of Pr^{3+} -doped transparent-glass-ceramic containing $\text{Ca}_5(\text{PO}_4)_3\text{F}$ nanocrystals, *J. Am. Ceram. Soc.* 96 (2013) 3569–3575.
- [58] D. Rajesh, R.J. Amjad, M. Reza Dousti, A.S.S. de Camargo, Enhanced VIS and NIR emissions of Pr^{3+} ions in TZYn glasses containing silver ions and nanoparticles, *J. Alloy. Compd.* 695 (2017) 607–612.
- [59] C.R. Kesavulu, H.J. Kim, S.W. Lee, J. Kaewkhao, N. Wantana, S. Kothan, S. Kaewjaeng, Optical spectroscopy and emission properties of Ho^{3+} -doped gadolinium calcium silicoborate glasses for visible luminescent device applications, *J. Non-Cryst. Solids* 474 (2017) 50–57.
- [60] X. Fan, J. Wang, X. Qiao, M. Wang, J.L. Adam, X. Zhang, Preparation process and upconversion luminescence of Er^{3+} -doped glass ceramics containing Ba_2LaF_7 nanocrystals, *J. Phys. Chem. B* 110 (2006) 5950–5954.